Nasser M. El-Basiony*, Mostafa H. Sliem, Ali A. Abd-Elaal*,
Aboubakr M. Abdullah*, Noora H. Al-Qahtani, ElSayed. G. Zaki,
Paul C. Okonkwo, Salah S. Elyan and Samy M. Shaban*

Theoretical and experimental insights into the C-steel aqueous corrosion inhibition at elevated temperatures in 1.0 M HCl via multi-carbonyl Gemini cationic surfactants

Abstract: Despite corrosion being an inevitable process, researchers strive to control corrosion. In this study, our goal was to prepare two amido Gemini cationic surfactants, LAPG and MAPG, each with different alkyl chains and multiple carbonyl groups as rich electronic rich centers. We aimed to evaluate these surfactants as potential corrosion inhibitors for carbon steel (CS) in 1 M HCl at temperatures of $25–55 \pm 0.1\,°C$. In theoretical investigations, DFT parameters and Mont Carlo simulation were run to predict the adsorption affinity and reactive sites of the LAPG and MAPG molecules. Their efficacy was investigated experimentally considering weight loss and electrochemical techniques. The Tafel polarization revealed that at 0.1 mM of LAPG and MAPG, the corrosion current density (i_{corr}) of CS was reduced to the lowest extent (75.56 and 53.82 $\mu A\,cm^{-2}$) compared to 529.3 $\mu A\,cm^{-2}$ in the absence of the inhibitors. EIS data suggests the enhancement of the thickness of the adsorbed layers of the studied compounds from the decrease of the double-layer capacitance C_{dl} values. The Langmuir isotherm explained the adoption phenomena of these

*Corresponding authors: Nasser M. El-Basiony and Samy M. Shaban**, Egyptian Petroleum Research Institute, Nasr City 11727, Cairo, Egypt; and School of Chemical Engineering, Sungkyunkwan University, Suwon 16419, Republic of Korea, E-mail: n.elbasiony56@gmail.com (N. M. El-Basiony),
dr.samyshaban@yahoo.com (S. M. Shaban); **Ali A. Abd-Elaal**, Egyptian Petroleum Research Institute, Nasr City 11727, Cairo, Egypt, E-mail: ali_ashour5@yahoo.com; and **Aboubakr M. Abdullah**, Center for Advanced Materials, Qatar University, Doha P.O. Box 2713, Qatar, E-mail: bakr@qu.edu.qa
Mostafa H. Sliem and Noora H. Al-Qahtani, Center for Advanced Materials, Qatar University, Doha P.O. Box 2713, Qatar
ElSayed. G. Zaki, Egyptian Petroleum Research Institute, Nasr City 11727, Cairo, Egypt,
E-mail: chemparadise17@yahoo.com
Paul C. Okonkwo, School of Biotechnology, Badr University in Cairo, Badr City, Cairo 11829, Egypt
Salah S. Elyan, Mechanical and Mechatronics Engineering Department, College of Engineering, Dhofar University, Salalah, Oman

compounds at 25–55 ± 0.1 °C. Activation and adsorption thermodynamic parameters predicted the chemisorption behavior of these molecules onto the steel surface. AFM and XPS tools confirm the CS surface protection due to these inhibitors' adsorbed layer. A parallel study showed the superiority of these corrosion inhibitors in HCl compared with those reported earlier, making these compounds highly promising corrosion inhibitors, especially in high-temperature acidic environments.

1 Introduction

Many industrial applications use carbon steel (CS) as the main construction of their process due to its low cost, unique mechanical properties, and easy availability in the fabrication of vessels. Although carbon steel may be used in a variety of engineering fields, including oil and gas transportation, electricity production, desalination, food, and chemical and electrochemical industries, it is easy to be corroded in a variety of aggressive media, especially the acidic environments [1–3]. Knowing that many processes use acid solutions such as descaling, cleaning, oil well acidification, and petrochemical processes, several techniques have been employed to monitor and inhibit the corrosion processes in these media [4, 5]. For example, several inhibitors are added in small quantities to slow the internal corrosion of industrial equipment (pipelines, storage tanks, etc.) [6, 7]. These inhibitors are chemicals that can be physisorbed and/or chemisorbed onto a metal surface, forming a protective barrier layer against metal corrosion in aggressive environments. Corrosion inhibitors are the most feasible mitigation method due to benefits such as low cost, high efficiency, eco-friendly and wide use in various fields.

Surfactants consider kind of organic materials that have two parts of different polarities in the same skeleton [8, 9]. The unique nature of the surfactant enhances their adsorption at the interface at CS/aggressive medium by constructing a protective film. The surfactant exhibited high corrosion inhibition efficiency, safety, ease of use, and low manufacturing cost [10, 11]. The hydrophilic portion of the surfactant molecules enhances their adsorption on metallic surfaces, inhibiting their active sites and protecting the surfaces against corrosion [12–15]; additionally, they reject the polar aqueous phase through aggregating and associating their hydrophobic tails group [16]. Gemini surfactants is a kind surfactant with two amphiphilic moieties linked by a spacer group at or near two head groups. This unique structure render them with higher surface activity compared to individual surfactants [17, 18]. The Gemini surfactant have lower critical micelle concentrations (CMCs) and C_{20}, better solubilizing abilities, greater wetting, foaming, and lime-soap dispersing

properties, corrosion resistance, and stronger biological activities [19]. Due to government and environmental precautions, eco-friendly surfactants will replace the conventional ones, therefore the Gemini surfactant is favorable than traditional one.

Introducing easily cleavable bonds, such as ester and amid bonds, into surfactants is one approach to improve biodegradability. Geo et al., for example, reported the synthesis of Gemini surfactants with an ester bond on the spacer unit based on 1,2-bis-chloroacetoxy-ethane, which had strong foaming and emulsifying properties [20]. Surfactants containing ester linkages have been demonstrated to be biodegradable in numerous investigations [21–24]. Many studies have revealed that amide Gemini surfactants are biodegradable and sensitive to chemical/enzymatic hydrolysis [25]. Furthermore, the amide group improves the surfactants' physicochemical characteristics and enhances their performance [26].

Herein, we aimed to synthesize organic Gemini cationic surfactant having multiple functional groups that act as electronic rich functional groups for an enhanced corrosion inhibitor. We designated that Gemini cationic surfactants having multi-carbonyl as well as others groups a new surfactant structure for providing higher adsorption centers. Few papers in literature that handled that kind of Gemini cationic surfactant as corrosion inhibitors. We used two Gemini cationic surfactants (LAPG and MAPG) as corrosion inhibitors for CS in a highly acidic medium (1 M HCl) at room and elevated temperatures. We employed density functional theory (DFT) and Monte Carlo (MC) simulation approaches to determine the quantum chemical parameters of several surfactants and predict their adsorption behavior. We then examined the impact of these surfactants on electrochemical kinetics parameters using gravimetric and electrochemical test methods. Additionally, we conducted surface analysis studies using Atomic Force Microscopy (AFM) and X-ray photoelectron spectroscopy (XPS) to further understand the surfactants' effects. The novelty of this work is not only using these surfactants as corrosion inhibitors, which has never been done before, but their inhibition efficiencies increase as the temperature increases, which is an outstanding behavior. This differs from most corrosion inhibitors, whose functionality is based on their adsorption mechanism on metallic surfaces. Also, the thermodynamic parameters for the adsorption of these inhibitors have been calculated and reported. The adsorption was found to be chemical and followed the Langmuir adsorption isotherm.

2 Experimental

2.1 Chemicals and solutions

1 M of hydrochloric acid was selected as an aggressive medium. It was prepared by diluting a concentrated HCl using bi-distilled water. Two amido Gemini surfactants with the chemical structure
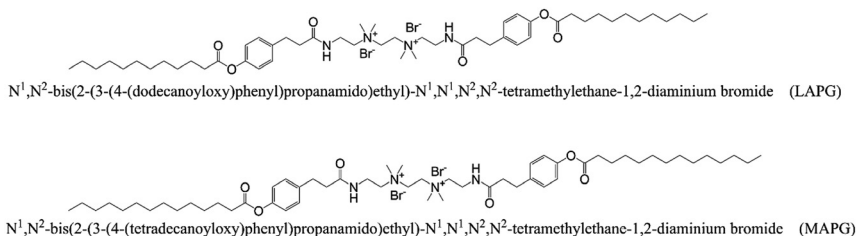
N^1,N^2-bis(2-(3-(4-(dodecanoyloxy)phenyl)propanamido)ethyl)-N^1,N^1,N^2,N^2-tetramethylethane-1,2-diaminium bromide   (LAPG)

N^1,N^2-bis(2-(3-(4-(tetradecanoyloxy)phenyl)propanamido)ethyl)-N^1,N^1,N^2,N^2-tetramethylethane-1,2-diaminium bromide   (MAPG)

Figure 1: The chemical structure for the two as-synthesized amide Gemini cationic surfactants.

in Figure 1 have been formulated as previous work [27]. The CS specimens used in our investigation have a composition of 0.2 % C, 0.6 % Mn, 0.05 % S, 0.04 % P, and 0.003 % Si while the rest is Fe. The used CS specimens of a dimension of $60 \times 30 \times 3$ mm^3 were involved in the weight loss measurements. In contrast, the electrochemical measurements were conducted using a cylinder shape steel with 0.5 cm^2 as contacting surface area.

2.2 Quantum chemical study

The calculated parameters output from quantum chemical studies of the prepared amido Gemini cationic LAPG & MAPG surfactants predict the inclination of LAPG & MAPG to act as corrosion inhibitors for iron alloy. DMol3 module in Material studio 6.0 software has executed these theoretical studies using GGA with BOP method with a 3.5 DNP basis set as reported in our previous work [28, 29]. The probability of amido Gemini cationic LAPG & MAPG surfactants to be adsorbed over iron alloy is simulated via the adsorption locator module implemented in Ms6.0 software. Monte Carlo simulation (MC) process of LAPG & MAPG over Fe (110), the most stable plane of iron, in the presence of 500 H$_2$O molecules, is running in simulation box $74.47 \times 74.47 \times 30.05$ A. The simulated process options for LAPG & MAPG + 500 H$_2$O/Fe (110) annealing were adjusted where the total annealing steps were 105,000 steps (7 cycles and 15,000 steps per cycle), geometry optimization of the whole system was done at smart algorithm with a medium level of convergence (energy 1×10^{-3} kcal/mol and force 0.5 kcal/mol/A), and the summation method for electrostatic and Van der Waals was atom based with cut off distance 12.5 A.

2.3 Weight loss test method (WL)

The corrosion inhibition performance of the two Gemini cationic surfactants-based amido structures (LAPG and LAPG) had been investigated gravimetrically against the CS corrosion in aggressive HCl solution (1.0 M). The weight loss measurements were conducted at four different temperatures 25, 35, 45, and 55 ± 0.1 °C, in a water bath to control the temperature. Before starting each run, all coupon specimens were abraded using different grades of emery papers (400–2000), washed with distilled water, then acetone before drying. Each sample was weighed before and after immersing in the aggressive solution without and with different concentrations of LAPG and LAPG individually for 24 h using a highly precious digital balance.

2.4 Electrochemical techniques (ETs)

ETs, including electrochemical impedance spectroscopy (EIS) and potentiodynamic polarization (PDP), were performed via a 3-electrode system using a GAMRY 3000 potentiostat/galvanostat/ZRA (Warminster, PA, USA). For controlling the temperature, the ETs were done in a double-jacketed Pyrex cell attached to a Julabo F12 thermostat (GmbH, Seelbach, Germany). The working electrode is a disc of CS with a 0.5 cm^2 exposed area; a saturated calomel electrode (SCE) and a platinum wire were utilized as a reference and a counter electrode, respectively. The ETs were conducted after 30 min of immersion of the bare steel into 1 M HCl (see Figure S1). EIS measurements were studied in a frequency range of 100 kHz–0.1 Hz with a 10 mV AC amplitude. PDP curves were investigated within a potential window of –0.5 to 0.01 V versus the open circuit potential (OCP) with a scan rate of 0.167 mV/s. The LAPG and MAPG corrosion inhibitors were prepared with varying concentrations of 1×10^{-6}, 5×10^{-6}, 1×10^{-5}, 5×10^{-5}, and 1×10^{-4} M in 1 M HCl to study their inhibition effect against CS corrosion. Each test was repeated twice, and the mean values were reported.

2.5 Surface analysis (AFM & XPS)

An atomic force microscope (AFM, Asylum Research MFP-3D, Santa Barbara, CA, USA) was used to (i) study the surface topography of CS after 24 h exposure in inhibitor-free HCl, and after LAPG and MAPG optimum concentration addition was added and to (ii) measure the surface roughness. The CS surface treated with 1×10^{-4} MAPG has been examined using X-ray photoelectron spectroscopy (XPS). XPS was performed using an Al-Kα excitation source and operating at a constant 1486.7 eV. The analyzer energy mode was 10 mA for the target current, 50 eV for the pass energy, and 2.4 nm s^{-1} for sputtering speed. The angle between the sample and the ion gun was 30°. The uncertainty in binding energy was 0.1 eV C1s peak at 284.6 eV was observed for all the obtained spectra. The spectral simulation for the peaks from experiments was obtained using Kratos Advantage software, where the XPS standard spectral line data were derived from the XPS manual.

3 Results and discussions

3.1 Quantum chemical study

The collected snapshots presented in Figure 2 display the most stable distributed atomic structure of amido Gemini cationic LAPG & MAPG surfactants in space (optimized geometry structure), frontier molecular orbitals, electrostatic potential mapping, and electron density distribution over the LAPG & MAPG structures. The electron density distributed over the quaternary nitrogen and bromide atoms in the highest occupied molecular orbitals (HOMO) indicates the probability of LAPG & MAPG adsorption via electron donation to the empty outer orbital of iron (3d), and electrostatic attraction with the charged iron surface make the studied LAPG & MAPG coming closer to the iron surface. Also, the electron cloud distributed over ester, amid, and phenyl groups in the lowest unoccupied molecular orbitals (LUMO) allows the electron

back-donation transfer from the outer fulfilled orbitals (4s and 3d) of iron to the anti-bonding molecular orbital (π^*) of LAPG & MAPG. The electron donation and receiving process gives the prepared LAPG & MAPG a high propensity to be preferable corrosion inhibition ability for iron. Electrostatic potential maps for LAPG & MAPG certain the HOMO and LUMO point of view. The regions with red color pointed to high electron density, while the blue one indicates low electron density. These regions (red and blue) are considered adsorption centers. The electron density over the long aliphatic chains gives LAPG & MAPG probability to form a dense and more compacted adsorbed layer over the iron surface [30–32]. The numerical analysis of DFT parameters based on energy values of HOMO and LUMO calculated according to the following equations and recorded in Table 1:

$$\Delta E_{\text{gap}} = E_{\text{LUMO}} - E_{\text{HOMO}} \tag{1}$$

$$\eta = \frac{E_{\text{LUMO}} - E_{\text{HOMO}}}{2} \tag{2}$$

$$\sigma = \frac{1}{\eta} \tag{3}$$

$$\chi = \frac{-(E_{\text{HOMO}} + E_{\text{LUMO}})}{2} \tag{4}$$

$$E_{\overleftarrow{\text{back–donat.}}} = -\frac{\eta}{4} \tag{5}$$

$$\Delta N = \frac{(\varphi_{Fe} - \chi_{cat.surf.})}{[2(\eta_{Fe} + \eta_{cat.surf.})]} \tag{6}$$

where: energy gap (ΔE_{gap}), global hardness (η) and softness (σ), electronegativity (χ), electron back-donation ($\Delta E_{\text{back-d}}$), the fraction of transferred electron (ΔN) and Work function (φ) of Fe (110) plan is 4.82 eV [33, 34].

According to the data recorded in Table 1, the values of E_{HOMO}, E_{LUMO}, and ΔE_{gap}, for both studied compounds LAPG & MAPG indicate that they may have adsorption propensity compared to the previously published compounds [27]. The electron donation and acceptance are related to the E_{HOMO} and E_{LUMO} values, respectively. It can be noticed that E_{HOMO} follows the order MAPG > LAPG. This indicates that MAPG has a high affinity to donate to the empty 3d orbital electron compared to LAPG and, in turn, has a high probability for adsorption affinity over the CS surface. On the other side, MAPG has a lower value (high negative) of E_{LUMO} compared to LAPG, indicating the high acquiring affinity to the liberated electron from fulfilled 3d or/and 4S orbitals of iron also helps the adsorption process perform efficiently via the back-donation process. The adsorption activity of MAPG & LAPG is related to the energy
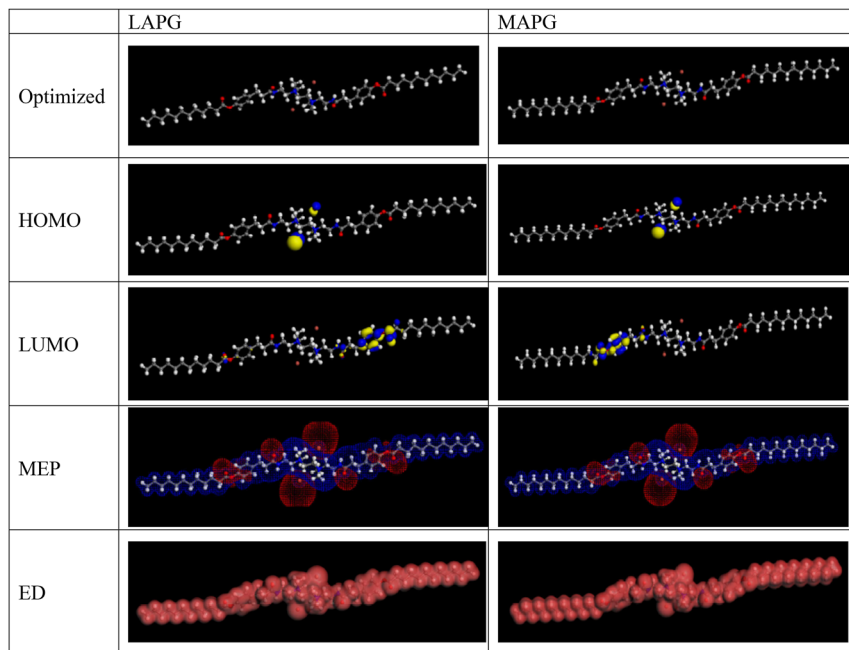
Figure 2: Optimized geometry structures, FMOs (HOMO & LUMO) and molecular electrostatic potential map (MEP) of the studided cationic surfactants (LAPG & MAPG).

Table 1: Quantum chemical parameters of the investigated LAPG, and MAPG surfactant compounds.

Compound	E_H (eV)	E_L (eV)	ΔE (eV)	χ (eV)	η (eV)	$\Delta N_{(110)}$	$E_{\overleftarrow{\text{back−donate}}V}$	μ (Deby)
LAPG	−4.129	−1.375	2.754	2.752	1.377	1.542	−0.344	0.742
MAPG	−4.117	−1.396	2.720	2.756	1.360	1.559	−0.340	0.460

difference between HOMO and LUMO (ΔE_{gap}). The lower ΔE_{gap} value is, the higher reactivity and tendency of adsorption are. According to the data recorded in Table 1, the adsorption performance of MAPG over CS is more energetically favored than LAPG. Also, the adsorption probability of studied compounds can be predicted from softness and hardness points of view. Soft molecules have a high reactivity tendency (low ΔE_{gap}) and, in turn, a high electron-donating ability. The MAPG and LAPG are soft molecules relative to the published molecules, but MAPG is more reactive than LAPG [35]. The numerical value of the dipole moment parameter gives insight into the probability of tested compounds accumulating and forming a protective layer

shielding the metallic surface from the offensive action of corrosive media. As we reported elsewhere, lowering dipole moment values encourages the accumulation of the tested molecules over the CS surface [36]. So, MAPG has an accumulation affinity higher than LAPG. This predicts the adsorption superiority of MAPG over the LAPG and is in touch with the previous discussion of quantum descriptors. An adsorption phenomenon involves sharing electrons between synthesized compounds and metal surfaces. This can be discussed based on ΔN and $E_{\overleftarrow{\text{back–donat.}}}$ values recorded in Table 1 according to Gomez theory [37]. Based on ΔN value, the electrons can transfer to the metal in case of $\Delta N > 0$ (positive) or vice versa when $\Delta N < 0$ (negative) [34]. The electron transfer process is related to the value of electronegativity (χ); the lower the electronegativity, the higher the electron transfer. The data in Table 1 confirm the capabilities of both compounds to transfer electrons to the CS surface. The MAPG has a higher positive ΔN value than LAPG, which will support the corrosion inhibition ranking prospected. Also, $E_{\overleftarrow{\text{back–donat.}}}$ values recorded in Table 1 support the high adsorption propensity of MAPG [33, 38].

3.2 Monte Carlo simulations (MCs)

MC simulation has a significant role in simplifying and visualizing the adsorption of the under-studied compounds over the most stable plan of ion crystal Fe (110). This helps in predicting the inhibition affinity of specific compounds. The optimized geometric configurations and the orientations of the under-investigation compounds over Fe (110) are obtained from the simulated annealing process at certain adjusted conditions, as represented in Figure 3. The inspection of Figure 3(a) and (b) reflects the capabilities of both compounds to be adsorbed on the plane of Fe (110) because their active adsorption centers (HOMO & LUMO) are oriented flat over (as seen from top views) and parallel to (from side views) the Fe (110) surface. These orientations make the donor-acceptor interaction take place efficiently, and the exposed metallic surface area becomes most diminutive as possible. The output calculated data of MC recorded in Table 2 can be summarized as follow:

 i. The large negative adsorption energy values for the tested compounds with Fe (110) predict their strong and spontaneous adsorption affinity [39].
 ii. The absolute values of E_{ads} for MAPG & LAPG suggest that MAPG has more favorable adsorption efficacy than LAPG.
iii. The tested cationic compounds have an affinity to replace the adsorption water molecules from the CS surface and form a stable barrier adsorption film saving the CS from the severity of surrounding media as their E_{ads} values are higher than water adsorption energy [37, 40].
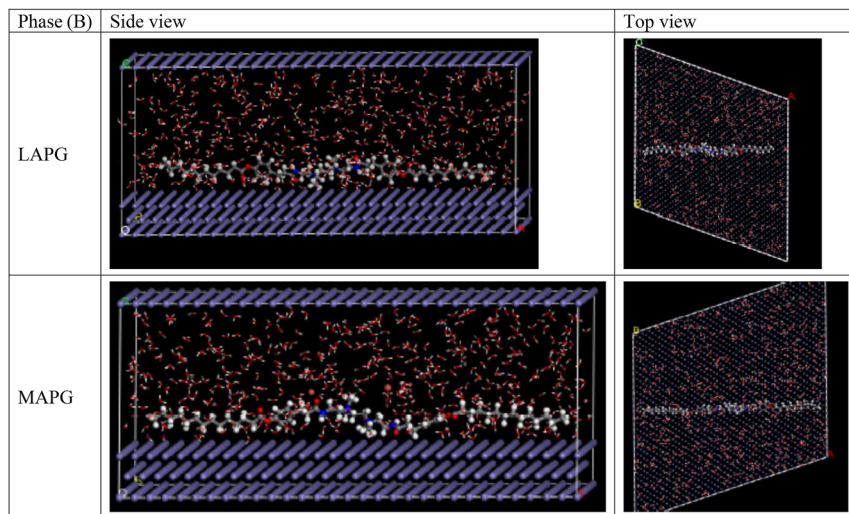
Figure 3: Side and top snapshot views of the most stable adsorption configuration of Fe (1 1 0)/LAPG & MAPG +500 H$_2$O.

Table 2: The outputs energies calculated by Monte Carlo simulation for LAPG, and MAPG catonic-surfactant compounds solvent phase on Fe (110).

Compound	E_T (kJ/mol)	E_{ads} (kJ/mol)	$E_{rig.ads}$ (kJ/mol)	$E_{def.}$ (kJ/mol)	(dE_{ads}/dNi) (kJ/mol)	
					Catonic-surf	H$_2$O
LAPG + 500 H$_2$O	−24,730.39	−34,371.40	−25,359.85	−9011.56	−1058.76	−62.2946
MAPG + 500 H$_2$O	−24,857.76	−34,986.97	−25,506.27	−9480.70	−1609.61	−61.44

It is evident that DFT and MC indices recorded in Tables 1 and 2 suggest the under-studied cationic surfactant compounds (MAPG & LAPG) have a high probability of being adsorbed firmly over iron surface via hetero atoms of ester amid and quaternary ammonium salt groups and π-electrons of phenyl groups. And this makes the prepared compounds have high potential applications as corrosion inhibitors.

3.3 Gravimetric analysis

The corrosion inhibition efficiency (η_w) & the surface coverage (θ) conducted by the synthesized amido Gemini cationic (LAPG & MAPG) surfactant-inhibitors have been investigated by weight loss technique according to Equations (7) and (8) [41]:

$$\%\eta_w = \left(\frac{CR^o - CR}{CR^o}\right) \times 100 = \theta \times 100 \qquad (7)$$

$$CR = \frac{W}{St} \qquad (8)$$

where CR and CR^o refer to the corrosion rate of CS immersed in the aggressive 1.0 M HCl with different concentrations of the LAPG and MAPG and without, respectively. The $t = 24$ h as immersion time. The CR assigned, based on Equation (8), W and S to steel loss in mg and the exposed steel surface area in cm^2. Table 3 shows the η_w and CR of steel corrosion in the absence and presence of different concentrations of the LAPG and MAPG amido Gemini surfactant-inhibitors at 25, 35, 45, & 55 °C. As the inhibitor concentration increases, the weight loss of the CS specimen also decreases, confirming the steel protection. Reducing weight loss and, subsequently, the CR refers to adsorption of the prepared amido Gemini surfactant on surfactants on the steel surface. The adsorption of LAPG and MAPG on the surface leads to forming of a protective layer that isolates the steel surface and the aggressive solution. Increasing the inhibitor concentration led to increasing the amount of the LAPG and MAPG adsorbed on the steel surface, hence increasing the θ and so enhancing the steel protection η_w. Additionally, the weight loss results in Table 3 clarify the potential impact of the hydrophobic surfactant tail on the inhibition efficiency performance. Increasing the hydrophobic tail length led to an increase in steel inhibition efficiency. For an instant, the η_w of LAPG, and MAPG at 25 °C, are equal to 88.01 and 90.1 % at the concentration of 1×10^{-4} M, respectively Table 3. As clarified previously, their adsorption affinity on the surfaces increases with the elongation of the surfactant tail [9, 42]. Subsequently, the surfactant tail controls the adsorption of the surfactant inhibitor on the surface, increasing the surface coverage & inhibition efficiency [43, 44]. Increasing the solution temperature that contains the synthesized LAPG, and MAPG Surfactant inhibitor, the corresponding η_w increases as clarified from the experimental results depicted in the Table 3. The behavior of increasing η_w of the LAPG, and MAPG solution with raising the solution temperature reflects their chemical adsorption on the steel surface. Increasing solution temperature induces some chemical structure change that promotes electron densities of the active centers, subsequently enhancing the adsorption on the corroded steel surface [45–47]. The two positively ammonium-charged centers of the LAPG and MAPG amido Gemini cationic surfactant electrostatically interact with the negative center generated on the steel surface dipped in the aggressive acidic medium [48].

The Arrhenius-type plot was conducted according to Equation (9) to determine the apparent activation energy (E_a) to elucidate the corrosion kinetics.

Table 3: Corrosion rate, surface coverage and percentage inhibition efficiency for carbon steel in different concentrations of LAPG, and MAPG surfactants at different temperatures.

| Temp. (°C)	Inhibitor conc (M)	LAPG				MAPG			
		Weight loss (mg)	K (mg cm^{-2} h^{-1})	Θ	η (%)	Weight loss (mg)	K (mg cm^{-2} h^{-1})	Θ	η (%)
25	0	411.3	0.3662	–	–	411.3	0.3662	–	–
	1×10^{-6}	137.3	0.1222	0.6662	66.62	128	0.1140	0.6888	68.88
	5×10^{-6}	114.7	0.1021	0.7211	72.11	106.9	0.0952	0.7401	74.01
	1×10^{-5}	84.9	0.0756	0.7936	79.36	74	0.0659	0.8201	82.01
	5×10^{-5}	68	0.0605	0.8347	83.47	55.5	0.0494	0.8651	86.51
	1×10^{-4}	49.3	0.0439	0.8801	88.01	40.8	0.0363	0.9008	90.08
35	0	832	0.7407	–	–	832	0.7407	–	–
	1×10^{-6}	241.3	0.2148	0.7100	71.00	222.98	0.1985	0.7320	73.20
	5×10^{-6}	216	0.1923	0.7404	74.04	187.2	0.1667	0.7750	77.50
	1×10^{-5}	151.6	0.1350	0.8178	81.78	129.8	0.1156	0.8440	84.40
	5×10^{-5}	102.4	0.0912	0.8769	87.69	87.4	0.0778	0.8950	89.50
	1×10^{-4}	79	0.0703	0.9050	90.50	70.6	0.0629	0.9151	91.51
45	0	1580	1.4067	–	–	1580	1.4067	–	–
	1×10^{-6}	426.6	0.3798	0.7300	73.00	402.9	0.3587	0.7450	74.50
	5×10^{-6}	347.6	0.3095	0.7800	78.00	303.3	0.2700	0.8080	80.80
	1×10^{-5}	260.4	0.2318	0.8352	83.52	198.4	0.1766	0.8744	87.44
	5×10^{-5}	162.7	0.1449	0.8970	89.70	126.4	0.1125	0.9200	92.00
	1×10^{-4}	115	0.1024	0.9272	92.72	99.5	0.0886	0.9370	93.70
55	0	2988	2.6603	–	–	2988	2.6603	–	–
	1×10^{-6}	687	0.6116	0.7701	77.01	599.6	0.5338	0.7993	79.93
	5×10^{-6}	541.5	0.4821	0.8188	81.88	487.14	0.4337	0.8370	83.70
	1×10^{-5}	353.7	0.3149	0.8816	88.16	292.82	0.2607	0.9020	90.20
	5×10^{-5}	228.9	0.2038	0.9234	92.34	169.4	0.1508	0.9433	94.33
	1×10^{-4}	156.4	0.1392	0.9477	94.77	116.9	0.1041	0.9609	96.09
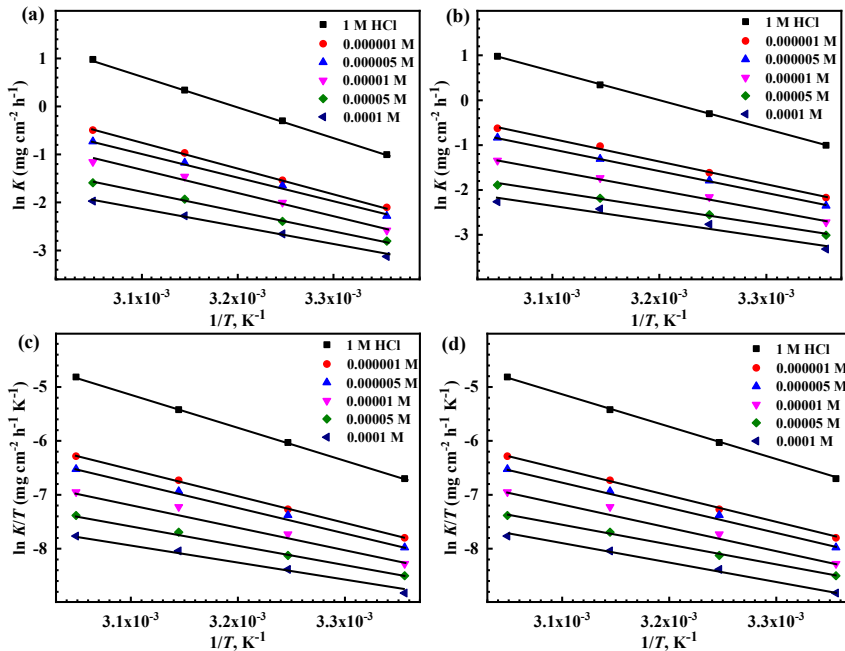
Figure 4: Arrhenius plots (a, b) and transition state plots (c, d) for carbon steel dissolution in absence and presence of different concentrations from LAPG, MAPG.

$$k = A \exp\left(\frac{-E_a}{RT}\right) \tag{9}$$

where the k corresponds to the corrosion rate, A is the Arrhenius constant, T is Kelvin temperature, and R corresponds to the gas constant [49]. The synthesized amido Gemini cationic surfactants LAPG and MAPG followed the Arrhenius plot, as shown in Figure 4a, with high regression coefficient. The E_a was extracted from the Arrhenius line slope that equals ($-E_a/R$). The E_a inspected in Table 4 in the presence of the synthesized amido Gemini cationic surfactants LAPG and MAPG are lower than in their absence (Blank solution), which reflects the chemisorption nature of the synthesized LAPG and MAPG inhibitors on the carbon steel surface [49, 50].

The activation entropy (ΔS^*) and Enthalpy (ΔH^*) were extracted from transition state theory (Equation (10)) [51]

$$\ln\left(\frac{k}{T}\right) = \left(\ln\left(\frac{R}{N_A h}\right) + \left(\frac{\Delta S^*}{R}\right)\right) - \frac{\Delta H^*}{RT} \tag{10}$$

Table 4: Activation parameters values of carbon steel in 1.0 M HCl of different concentrations of the synthesized LAPG, and MAPG surfactants inhibitors.

Inhibitor name	Conc. of inhibitor (M)	E_a (kJ mol^{-1})	Linear regression coefficient	ΔH^* (kJ mol^{-1})	ΔS^* (J mol^{-1} K^{-1})
LAPG	0	53.61	0.999	51.01	−82.17
	1×10^{-6}	43.95	0.9996	41.35	−123.71
	5×10^{-6}	41.82	0.9965	39.22	−132.04
	1×10^{-5}	39.34	0.9888	36.74	−142.81
	5×10^{-5}	33.40	0.9981	30.80	−164.96
	1×10^{-4}	31.29	0.9951	28.69	−174.41
MAPG	0	42.55	0.9965	39.95	−128.88
	1×10^{-6}	40.96	0.9997	38.36	−135.74
	5×10^{-6}	37.08	0.9964	34.49	−151.58
	1×10^{-5}	30.30	0.9954	27.70	−176.78
	5×10^{-5}	28.66	0.9549	39.95	−184.36

N_A & k, and h are assigned for Avogadro's number, metal dissolution rate, and Planck's constant, respectively. The transition state Equation (4) is represented in Figure 4b, with an intercept of $\log\left(\frac{R}{N_A h}\right) + \left(\frac{\Delta S^*}{R}\right)$ and a slope of $\left(\frac{\Delta H^*}{R}\right)$, that is used for calculating the corresponding ΔS^* and ΔH^*, respectively, as depicted in Table 4. The calculated positive values of ΔH^* refer to the endothermic nature of the corrosion process [52]. The determined ΔS^* values in the presence and LAPG, and MAPG inhibitors, Table 4, are negative, suggesting that the activated complex (rate-determining step) is an association rather than dissociation, i.e., more order conducted ongoing from reactant to activate complex [53–55].
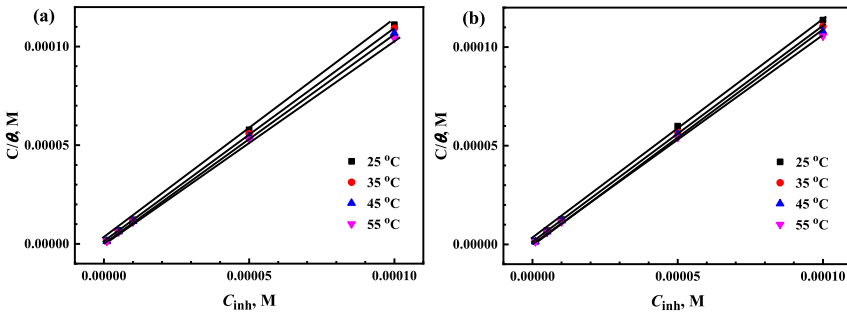
To investigate the adsorption behavior of the synthesized LAPG, and MAPG surfactants on the steel surface under the examined corrosion conditions, we performed several adsorption isotherms based on the θ values obtained from the weight loss experiment, such as Freundlich and Temkin (see Figure S2, Tables S1 and S2) while, Langmuir isotherm was the more fitted one. Our results, as shown in Table 5 and Figure 5, indicate that the Langmuir isotherm (Equation (11)) accurately describes the adsorption of the investigated inhibitors, with a high correlation coefficient (R^2) ~ 0.999.

$$\frac{C}{\theta} = \left(\frac{1}{K_{ads}}\right) + C \tag{11}$$

The K_{ads} (adsorption equilibrium constant) values have been extracted (Table 5) from the intercept of the Langmuir curve, which reflects the strong adsorption of all

Table 5: Thermodynamic parameters from Langmuir adsorption isotherm on carbon steel surface in 1.0 M HCl in presence of LAPG, and MAPG surfactants.

Inhibitor name	Temp. (°C)	Slope	R^2	$K_{ads} \times 10^{-5}$ (M^{-1})	ΔG_{ads} (kJ mol^{-1})	ΔH_{ads} (kJ mol^{-1})	ΔS_{ads} (kJ mol^{-1} K^{-1})
LAPG	25	1.13	0.9999	7.69	−43.55		0.1905
	35	1.10	0.9999	9.15	−45.46	13.24	0.1865
	45	1.07	0.9999	9.74	−47.10		0.1858
	55	1.05	0.9999	12.99	−49.36		0.1871
MAPG	25	1.11	0.9999	8.81	−43.89		0.1961
	35	1.09	0.9999	11.67	−46.08	14.57	0.1892
	45	1.06	0.9999	13.62	−47.99		0.1893
	55	1.04	0.9999	15.15	−49.78		0.1890

Figure 5: Langmuir isotherm adsorption model by the synthesized amido Gemini cationic surfactant (a) LAPG, and (b) MAPG on the steel surface at different temperatures.

synthesized LAPG and MAPG surfactant inhibitors on the steel surfaces. We observed increasing the K_{ads} as a function of increasing the solution temperature and the length of the surfactant tail, which matches their inhibition performance depicted in Table 3. This trend refers to the chemical adsorption mechanism of the LAPG and MAPG surfactant on the surface of the CS [56, 57].

The adsorption-free energy change (ΔG^o_{ads}) regarding the prepared amido Gemini cationic LAPG and MAPG surfactant inhibitors was calculated according to Gibbs equation (Equation (12)) [58, 59]:

$$\Delta G_{ads}° = -RT \ln\left(55.5 K_{ads}\right) \qquad (12)$$

The adsorption heat change (ΔH^o_{ads}) is extracted from the slope of Van't Hoff equation (Equation (13)), R is gas constant, and T is the temperature in Kelvin [60]:

$$\ln K_{\text{ads}} = \left(\frac{-\Delta H_{\text{ads}}°}{RT} \right) + \text{Constant} \tag{13}$$

The standard adsorption entropy ($\Delta S°_{\text{ads}}$) is calculated based on Equation (14) [52, 61]:

$$\Delta G_{\text{ads}}° = \Delta H_{\text{ads}}° - T\Delta S_{\text{ads}}° \tag{14}$$

The thermodynamic parameters $\Delta G_{\text{ads}}°$, $\Delta H_{\text{ads}}°$, and $\Delta S_{\text{ads}}°$ of LAPG and MAPG inhibitors were depicted in Table 5. The calculated $\Delta G°_{\text{ads}}$ values range from −43.55 to −49.78 kJ mol^{-1}, which give insight into the affinity of the synthesized LAPG, and MAPG surfactant to adsorb chemically on the steel surface under the examined condition of acidity and temperature conditions. The chemical adsorption by the LAPG and MAPG surfactant involves electron transfer from their active centers to the vacant 3d-orbital of iron under inspected temperatures 25–70 °C with, generating a coordination bond [62]. The positive values of the $\Delta H°_{\text{ads}}$ describe the endothermic nature of the process of LAPG and MAPG surfactant adsorption. The positive sign of $\Delta S°_{\text{ads}}$ values (Table 5) reflects more disorder due to replacing more than one H_2O molecule due to the LAPG and MAPG surfactant adsorption on CS surface [63].

The amido Gemini LAPG and MAPG surfactants under investigation contain numerous active adsorption centers that facilitate their adsorption onto the steel surface and promote their effectiveness as a corrosion inhibitor. Various functional groups, such as oxygen, nitrogen, C–O, C=C, C=O, and an aromatic structure, have been identified to enhance the adsorption process. The positively charged ammonium group can electrostatically interact with the cathodic sites that form on the surface of mild steel exposed to corrosive solutions. Additionally, the two hydrophobic tails of the synthesized inhibitors form a protective layer that insulates the contact between the steel surface and the aggressive medium.

3.4 Electrochemical impedance spectroscopy (EIS)

EIS technique has been utilized to investigate the electrode/electrolyte interactions and estimate their different corrosion mechanisms [64]. Figure 7 represents a simple one-time constant equivalent circuit commonly used to explain a uniform corrosion hypothesis. The elements of equivalent circuits are solution-resistant (R_s), charge transfer resistance (R_{ct}) and constant phase element of charge transfer process (*CPE*). It is worth mentioning that the double layer between the charged metal surface and the solution concerns an electrical capacitor. The capacitance of the double layer (C_{dl}) replaced by *CPE*. Because the non-ideal behavior of capacitance can be attributed to the roughness of the electrode interface or/and a non-uniform surface coverage or current distribution or corrosion rate.

The *CPE* is derived from the equation below [65, 66]:

$$Z_Q = [Y_0 (jw)^n]^{-1} \tag{15}$$

where Z_Q is the impedance for *CPE* (Ω cm^{-2}); Y_0 is the *CPE* constant as it is equal to the admittance of the system at unity (μs^n Ω^{-1} cm^{-2}); j is equal to $(-1)^{1/2}$, w is the angular frequency (rad s^{-1}), and the value of n ranges between 0 and 1. When $n = 1$, the *CPE* becomes equivalent to an ideal capacitor, and when $n = 0$, the *CPE* becomes equivalent to a resistor. The double-layer capacitance (C_{dl}) can be calculated using the equation below:

$$C_{dl} = \frac{(Y_0 * R_{ct})^{1/n}}{R_{ct}} \tag{16}$$

Figure 6 represents Nyquist and bode plots to display the behavior of CS immersed in acidic solutions treated and untreated with selected concentrations from the prepared corrosion inhibitors (LAPG, MAPG) at room temperature. The inspection of the Nyquist plot in Figure 6(a) and (c) reflects that the addition of the different inhibitors has no significant effect on the semicircular shape of EIS response curves except their diameter values. This means that the CS corrosion reaction mechanism is still
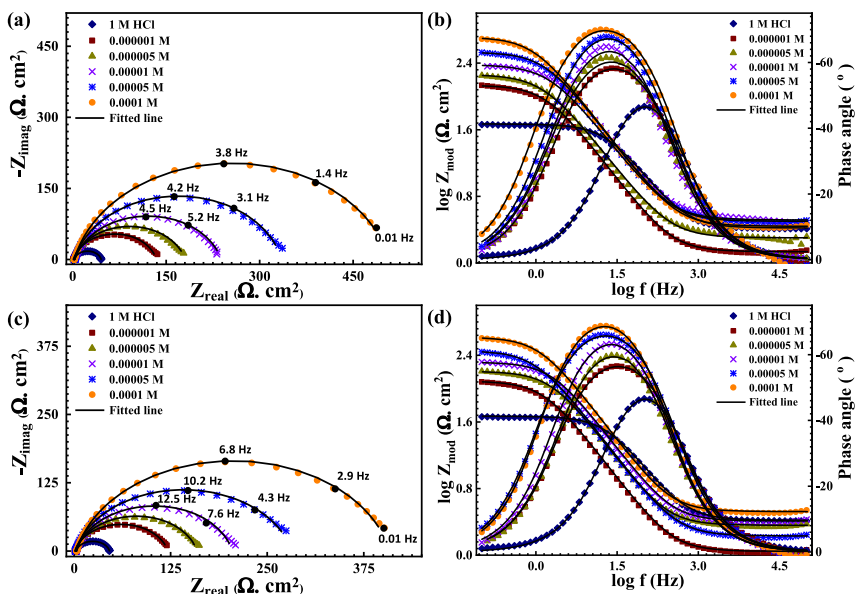

Figure 6: EIS Nyquist and Bode plots for the corrosion of carbon steel in 1.0 M HCl in the absence and presence of varied concentrations for (a, b) LAPG and (c, d) MAPG corrosion inhibitors at room temperature.

unchanged and controlled by the charge transfer process [67, 68]. The diameter of the capacitive loop in the Nyquist diagram is incremented with the inhibitors' addition, the absolute value of impedance Z_{mod} at lower frequency region in bode plot is raised to higher value and the phase angle at intermediate frequency area is shifted toward the more negative value. These observations may be related to the inhibition action of LAPG and MAPG compounds for CS corrosion, as their structures are enriched with the adsorption centers [69]. It can be observed that the capacitive loop looks like the depressed semicircle, and the calculated line slope of the Bode plot and phase angle values at the intermediate frequency region deviate from –1 to –90°, respectively, as reported in Table 6. This can be referred to as the frequency dispersion effect and the non-homogenous CS surface [70].

The electrochemical Impedance fitted parameters (R_s, R_{ct}, n, Y_o, C_{dl}, CPE) and the calculated surface coverage (θ) and inhibition efficiency $IE_{EIS}\%$ using equations are listed in Table 7.

$$\theta = \left(1 - \frac{R_{ct\,(blank)}}{R_{ct\,(inh.)}} \right) \tag{17}$$
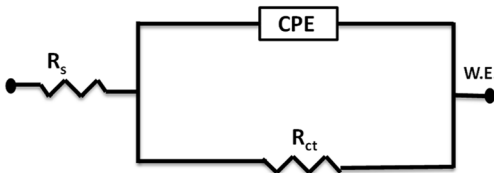

Figure 7: The equivalent circuit utilized for analyzing the measured EIS data.

Table 6: The slopes of the Bode impedance magnitude plots and the maximum phase angles (S) at definite frequency.

	Conc. M	(−) Slope	S (°) @ F (Hz)
Blank	0	0.659	−46.1@ 97.72
LAPG	1×10^{-6}	0.735	−58.2@ 26.30
	5×10^{-6}	0.746	−61.1@ 20.41
	1×10^{-5}	0.752	−64.8@ 19.49
	5×10^{-5}	0.765	−66.9@ 17.78
	1×10^{-4}	0.784	−70.1@ 15.48
MAPG	1×10^{-6}	0.772	−56.3@ 30.90
	5×10^{-6}	0.739	−59.4@ 27.54
	1×10^{-5}	0.734	−63.7@ 23.98
	5×10^{-5}	0.787	−66.0@ 19.49
	1×10^{-4}	0.765	69.1@ 16.98

$$IE_{EIS}\% = \theta \times 100 \qquad (18)$$

Table 7 shows that increasing the concentration of the different corrosion inhibitors enhances the numerical values of R_{ct} while suppressing the C_{dl} values. These may be due to the adsorption action of high electron density groups (oxygen atoms, quaternary nitrogen atoms, and amide groups) found in LAPG and MAPG and the long chain alkyl groups that increase the stability of adsorption film formed over CS. Adsorption of the synthesized compounds over the CS surface decreases the metal substrate's direct contact with the offensive action of HCl by replacing the adsorbed water and aggressive anions that lead to a decrease in the *CPE* values and increase the thickness of protective layer formed according to Helmholtz model.

$$\delta_{ads} = \frac{\varepsilon^* \varepsilon_o^* A}{C_{dl}} \qquad (19)$$

where δ_{ads} is the adsorbed layer thickness of the corrosion inhibitor, ε_o is the permittivity of air, ε is the local dielectric constant, and A is the electrode surface area. This equation shows that C_{dl} is inversely proportional to δ_{ads} i.e., the decrease of the C_{dl} value is attributed to the growth of the adsorbed film of corrosion inhibitor as its concentration increases in solution. It is evident from Table 7, n values are in the range of 0.723–0.892, representative non-ideal capacitive actions. Also, in the blank solution C_{dl} value of CS is more than that for an inhibited solution. The increment in corrosion inhibitors concentration reduces C_{dl} value. The decline in C_{dl} causes the regular replacements of water molecules via inhibitor molecule adsorption at CS/solution interface. The EIS reported parameters ended the ranking of the understudied cationic surfactants as LAPG < MAPG that coheres to the WL order.

Table 7: EIS parameters for the corrosion of carbon steel in 1.0 M HCl in the absence and presence of varied concentrations of LAPG, and MAPG surfactants at room temperature.

Inh.	C_{inh} (M)	R_S (Ω cm^2)	R_{ct} (Ω cm^2)	n	Y_0, μs^n (Ω^{-1} cm^{-2})	C_{dl} (μF cm^{-2})	θ	IE_{EIS} (%)
LAPG	0	2.46	41.93	0.723	460.2	101.40	–	–
	1×10^{-6}	2.48	122.7	0.767	259.7	91.16	0.6582	65.82
	5×10^{-6}	2.47	161.4	0.823	169.4	78.11	0.7402	74.02
	1×10^{-5}	2.77	213.9	0.841	133.1	67.91	0.8039	80.39
	5×10^{-5}	2.82	271.6	0.874	109.1	65.69	0.8456	84.56
	1×10^{-4}	2.40	407.3	0.892	84.29	56.03	0.8970	89.70
MAPG	1×10^{-6}	2.95	132.9	0.784	207.3	77.06	0.6844	68.44
	5×10^{-6}	2.05	176.7	0.796	172.6	70.56	0.7627	76.27
	1×10^{-5}	2.60	231.5	0.819	127.2	58.36	0.8188	81.88
	5×10^{-5}	2.62	337.8	0.862	93.31	53.64	0.8758	87.58
	1×10^{-4}	2.72	522.5	0.871	59.83	35.81	0.9197	91.97

3.5 Potentiodynamic polarization (PDP)

Figure 8 displays the electrochemical cathodic/anodic polarization of CS immersed in 1 M HCl in the absence and the presence of different concentrations of LAPG and MAPG corrosion inhibitors, respectively, under static conditions at room temperature.

Figure 8 shows that LAPG and MAPG corrosion inhibitors have no significant effect on the reaction mechanism of CS versus 1.0 M HCl, which saves the blank counterpart's polarization curves. The addition of LAPG and MAPG forces the CS polarization curve parts (cathodic and anodic) to be shifted toward the region of low corrosion rate compared to that of blank one, which indicates the inhibition ability of the prepared compounds (LAPG and MAPG) [71].

The extrapolation of i–v curves at Tafel regions gives rise to parameters used to evaluate the tested corrosion inhibitors and predict the reaction mechanism at the CS/HCl interface. These parameters: corrosion potential (E_{corr}), corrosion current density (i_{corr}), Tafel slopes (β_c and β_a), polarization resistance (R_P) are collected in Table 8. The polarization resistance can be derived using the Stern–Geary equation

$$R_P = \frac{\beta_c * \beta_a}{2.303 * i_{corr} * (\beta_c + \beta_a)} \tag{20}$$

Assuming that the whole surface of the CS is uniformly attacked, and no localized corrosion is detected, the corrosion rate could be derived from the equation below.

$$\text{corrosion rate (mpy)} = \frac{i_{corr} \times 10 \times M \times 3.15 \times 10^7}{F \times n \times d} \tag{21}$$

where i_{corr} is the corrosion current density (A cm^{-2}), 10 is a dimension change factor, M is the iron atomic weight (g mol^{-1}), 3.15×10^7 is the number of seconds in one year, F is the Faraday constant, n is the number of transferred electrons per metal atom, d is the density of iron.
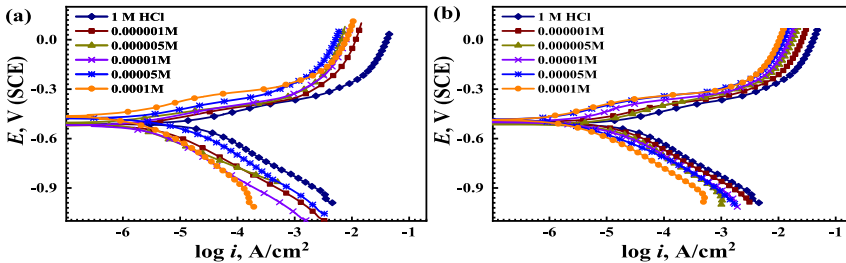

Figure 8: Potentiodynamic polarization curves for the corrosion of carbon steel in 1.0 M HCl in the absence and presence of varied concentrations for (a) LAPG and (b) MAPG corrosion inhibitors at room temperature.

Table 8: Potentiodynamic polarization parameters for corrosion of CS in 1.0 M HCl in the absence and presence of varied concentrations of LAPG & MAPG at room temperature.

Inh.	C_{inh} (M)	E_{corr} (mV$_{SCE}$)	i_{corr} (μA cm^{-2})	$-\beta_c$ (mV dec^{-1})	β_a (mV dec^{-1})	R_p (Ω cm^2)	Corrosion rate (mpy)	θ	IE_{pot} (%)
LAPG	0	−462	529.3	111.7	109.7	45.46	240.9	–	–
	1×10^{-6}	−454	181.9	103.9	107.2	126.1	82.78	0.6563	65.63
	5×10^{-6}	−473	156.4	126.2	111.1	164.2	71.18	0.7045	70.45
	1×10^{-5}	−471	122.3	135.1	105.7	210.8	55.66	0.7689	76.89
	5×10^{-5}	−470	101.5	165.9	101.5	269.7	46.19	0.8082	80.82
	1×10^{-4}	−479	75.56	178.6	113.9	400.7	34.38	0.8572	85.72
MAPG	1×10^{-6}	−461	169.1	108.3	106.9	138.3	76.96	0.6805	68.05
	5×10^{-6}	−486	140.4	122.5	98.24	168.8	63.90	0.7347	73.47
	1×10^{-5}	−468	99.82	115.1	105.7	239.9	45.43	0.8114	81.14
	5×10^{-5}	−490	77.49	166.3	102.8	356.4	35.26	0.8535	85.35
	1×10^{-4}	−474	53.82	179.2	97.51	510.1	24.49	0.8983	89.83

The calculated inhibition efficiency percentage (IE_{Pot}%) are functions of i_{corr} according to the equations:

$$IE_{Pot}\% = \frac{i_{corr}{}^{\circ} - i_{corr}}{i_{corr}{}^{\circ}} \times 100 \tag{22}$$

where the uninhibited and inhibited corrosion current densities are represented by $i_{corr}{}^{\circ}$ and i_{corr}, respectively.

The E_{corr} of CS in the presence of LAPG and MAPG fluctuated around that of blank by ±20 mV at varied concentrations. This means that the difference in CS potential in the absence and presence of the different studied corrosion inhibitors (LAPG and MAPG) and their concentrations are within the range of ±85 mV. This is reverted into the adsorbed molecules, which mask both anodic and cathodic reactions that take place at CS active centers (Fe → Fe^{+2} + 2e$^-$(anod) and 2e$^-$ + 2H$^+$ → H$_2$↑(cathod)). So, both corrosion inhibitors are classified as mixed corrosion inhibitors [72]. Intriguingly, adding LAPG and MAPG inhibitors leads to the suppression the i_{corr} of CS to 75.56 and 53.82 μA cm^{-2}, respectively, compared to blank counterpart 590 μA cm^{-2} and rise the inhibition efficacy to 85.72 and 89.83 %. These are returned into the high electron density centers presented in their chemical structure, forming a compact adsorbed film over the CS surface [73, 74]. This formed protective film increases the surface coverage (θ) up to 0.8572 and 0.8983, making the CS corrosion reaction hard to occur. Moreover, the CS polarization resistance (Rct) value is enhanced in the presence of LAPG and MAPG up to 407 and 510 Ω cm^2, respectively. This confirms the resistance stability of adsorbed inhibitors to form a barrier film that shields the CS surface away from the offensive action of hydrochloric acid media [75]. The PDP parameters arrange the performance of LGPA and MGPA like WL and EIS and comparing the tested inhibitors with their Gemini surfactants counterparts, showed a noticeable inhibition efficiency better than the other published materials at similar conditions (see Table S3).

3.6 Surface analysis studies

3.6.1 AFM analysis

The three-dimensional AFM technique has become one of the favorite choices for exploring surface topography at nano and micro levels. It is also a powerful method for elucidating the efficiency of the corrosion inhibitor at the metal/solution interface. The AFM technique provides sufficient images for quantitative analysis with nanoscale as it could explain the interaction mechanism between the steel surface and the other additives in the aggressive media. The surface roughness of carbon
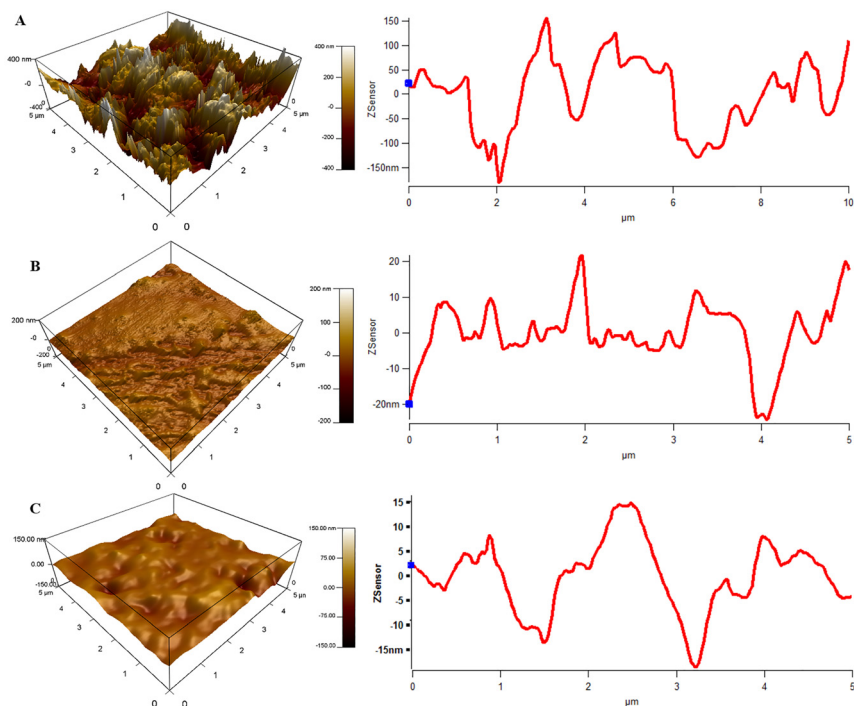
Figure 9: AFM images and height profile graphs for steel surface after immersion in 1.0 M HCl solution for 24 h in absence and presence of inhibitor at room temperature.

steel can be determined by the mean roughness factor (Ra). The R_a values show that the roughness of the metal surface immersed in 1.0 M HCl is around 132 nm. However, adding 0.0001 M of LAPG and MAPG corrosion inhibitor reduced the Ra to 16 and 8 nm respectively due to forming an adsorbed protective layer which shifted to reduce the surface roughness [43, 76]. Height profile graphs further support these results in Figure 9.

3.6.2 XPS analysis

The XPS analysis was utilized to identify the passivation layer formed on CS after immersion in 1.0 M HCl in the presence of 0.0001 M of MAPG corrosion inhibitor. The analysis revealed the presence of C1s, N1s, O1s, and Fe2p signals, as seen in Figure S3. The decomposition of each signal provides valuable information on the chemical environment of each element and, consequently, on changes in the chemical composition of the carbon steel surface, as shown in Figure 10. The carbon C1s signal
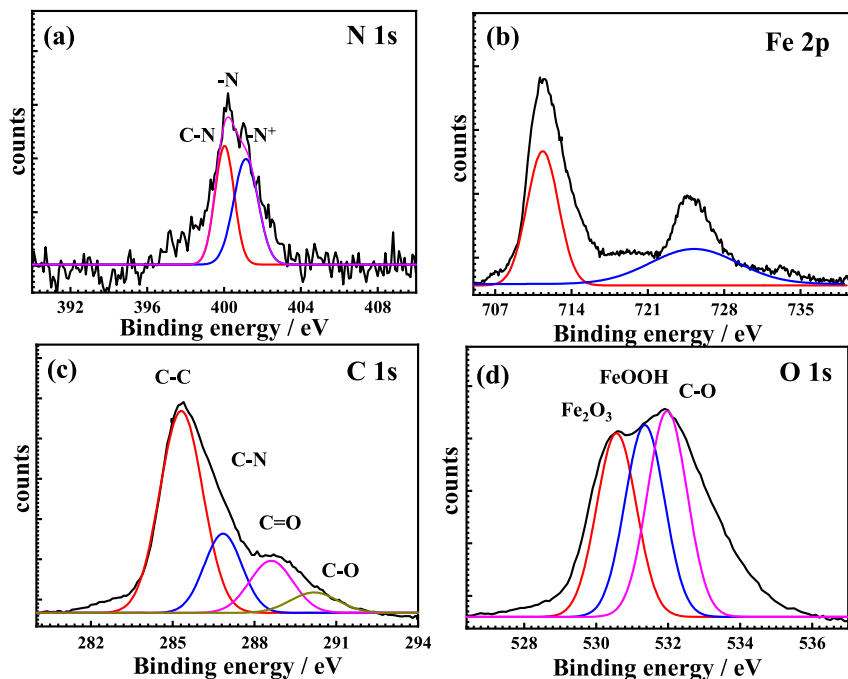
Figure 10: High resolution XPS spectrum of (a) nitrogen, (b) iron, (c) carbon and (d) oxygen atoms on the steel surface after immersion in 1.0 M HCl solution for 24 h in the presence of 0.0001 M of MAPG corrosion inhibitor at room temperature.
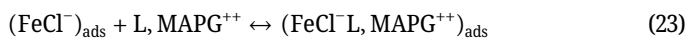
presents four peaks at 285; 286.69; 287.85, and 288.77 eV, respectively assigned to the carbon atoms of the groups (C–C and C–H), (C–N), (C=O) and (C–O), all belonging to the corrosion inhibitor. The deconvolution of the N1s signal provides three components, respectively at 399.50, 398.34, and 400.99 eV, related to the different types of nitrogen in the corrosion inhibitor (–N=, –N–, and N$^+$). The decomposition of the iron Fe2p signal essentially allows identifying any bonds between the metal substrate and the corrosion inhibitor. This deconvolution shows that iron exists in several forms: Fe–N at 707.10 eV, Fe$_3$O$_4$ at 708.45 eV, FeO at 709.80 eV, and FeOOH at 711.15 eV. Also, the deconvolution of the O1s signal gives rise to four peaks at 529.79; 530; 531.40, and 532.40 eV, respectively, corresponding to the same groups combining oxygen to iron, observed in the case of the Fe 2p signal: Fe$_2$O$_3$ and FeOOH. It can be concluded that the passivation layer is formed of oxides, hydroxides, and the adsorbed corrosion inhibitor.

3.7 Inhibition mechanism

The adsorption mechanism of organic compounds at metal/solution interfaces depends on more than one factor. We cannot ignore or specify one of them due to the complex nature of the adsorption process. These factors are the chemical structure of the inhibitor and the charge distribution overall in its structure in addition to the nature or/and charge of the steel surface [77]. Generally, corroded iron surface in HCl solution carries –Ve charge due to the electrostatic adsorption of Cl^- ions on the steel surface $(FeCl^-)_{ads}$.

So, we suggest the LAPG and MAPG adsorption follow one of these pathways or all of them:

1. Positive centers (quaternary nitrogen atoms or protonated oxygen atoms) attract physically with the negatively CS-charged centers according to [78]:

$$(FeCl^-)_{ads} + L, MAPG^{++} \leftrightarrow (FeCl^-L, MAPG^{++})_{ads} \tag{23}$$

$$(FeCl^-L, MAPG^{++})_{ads} \leftrightarrow (FeGL, MAPG^{++})_{ads} + Cl^- \tag{24}$$

2. The counter ions (bromide Br^-) synergist the action of Cl^- ions and attract with the Fe^{+2}.
3. The LAPG and MAPG form complex with the freshly generated Fe^{+2} over the CS surface according to the equation:

$$L, MAPG^{++} + Fe^{++} \leftrightarrow \left[[L, MAPG - Fe]^{+4} \right]_{ads} \tag{25}$$
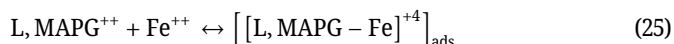
This complex attracts CS-charged surface, blocking the active centers of CS from reacting with HCl.

4. The aforementioned 1 and 3 pathways make the LAPG and MAPG compound come closer to the surface of CS and form a compact protected layer to shield the CS surface from the HCl contact.
5. Electron sharing between the electron-rich function groups in LAPG and MAPG compounds and the vacant 3d-orbital CS based on the donor-acceptor interaction concept forms a chemisorbed protective layer over the CS surface.

4 Conclusions

In this study, we investigated the use of Gemini cationic surfactants containing multiple carbonyl groups and different hydrophobic tails as corrosion inhibitors for CS in 1 M HCl at temperatures ranging from 25 to 55 $\pm$ 0.1 °C. The surfactants demonstrated high corrosion inhibition efficiency for CS, as confirmed through both theoretical and laboratory investigations using WL, EIS, and PDP techniques. DFT

and MCs calculated parameters predict the high adsorption inclination of LAPG and MAPG compounds over the CS surface. According to MCs, MAPG with 14 carbon as hydrophobic tail has a more spontaneous adsorption capability than LAPG with lower hydrophobic tail, outlining the significant role of the hydrophobic tail in control the corrosion inhibition efficiency. WL data show that the LAPG and MAPG decrease the CS corrosion rate to a high extent as their concentration increases at different temperatures. For the adsorption or/and thermodynamic activation parameters, both LAPG and MAPG surfactants exhibited a chemically adsorbed passive film that impedes CS corrosion reaction. The LAPG and MAPG follow the Langmuir adsorption isotherm model. The electrochemical data (Tafel and EIS) are in good coherence with each other and the WL data. E_{corr} slightly shifted negatively, indicating that LAPG and MAPG are mixed types. They prevent both the anodic and cathodic processes. i_{corr} decreases with rising LAPG and MAPG concentrations as well increasing the surfactant tail. These compounds addition leads to a rise in R_{ct} and a drop in Y°. And thus, lead to diminishing the contact surface area subjected to the offensive action of HCl. AFM and XPS confirms the protective layer formation over CS from the reduction of CS surface roughness.

Author contributions: All the authors have accepted responsibility for the entire content of this submitted manuscript and approved submission.
Conflict of interest statement: The authors declare no conflicts of interest regarding this article.

References

1. Wang X., Yang H., Wang F. A cationic Gemini-surfactant as effective inhibitor for mild steel in HCl solutions. *Corros. Sci.* 2010, *52*, 1268–1276.
2. Okonkwo P. C., Sliem M. H., Shakoor R. A., Mohamed A. M. A., Abdullah A. M. Effect of temperature on the corrosion behavior of API X120 pipeline steel in H2S environment. *J. Mater. Eng. Perform.* 2017, *26*, 3775–3783.
3. Madlangbayan M. S., Diola C. N. B., Tapia A. K. G., Peralta M. M., Peralta E. K., Almeda R. A., Bayhon M. A. L., Sundo M. B. Corrosion inhibition of sodium silicate with nanosilica as coating in pre-corroded steel. *Civ. Eng. J.* 2021, *7*, 1806–1816.
4. Frenier W. W., N. International. *Technology for Chemical Cleaning of Industrial Equipment*, 2001. http://app.knovel.com/hotlink/toc/id:kpTCCIE00R/technology-for-chemical.

5. Sliem M. H., Fayyad E., Abdullah A., Younan N., Al-Qahtani N., Nabhan F. F., Ramesh A., Laycock N., Ryan M., Maqbool M., Arora D. Monitoring of under deposit corrosion for the oil and gas industry: a review. *J. Petrol. Sci. Eng.* 2021, *204*, 108752.

6. El-Basiony N. M., Tawfik E., El-Raouf M., Fadda A., Waly M. Synthesis, characterization, theoretical calculations (DFT and MC), and experimental of different substituted pyridine derivatives as corrosion mitigation for X-65 steel corrosion in 1M HCl. *J. Mol. Struct.* 2021, *1231*, 129999.

7. Yadav M., Sliem M. H., Abdullah A. M., Youssef K. M., Al-Qahtani N. H. Impact of prolonged exposure to sour service on the mechanical properties corrosion mechanism of, nace carbon steel material used in wet sour gas multiphase pipeline. *Sustainability* 2022, *14*, 8015–8032.

8. Taha A. A., Shaban S. M., Fetouh H., Taha S. T., Sabet V., Kim D. H. Synthesis and evaluation of nonionic surfactants based on dimethylaminoethylamine: electrochemical investigation and theoretical modeling as inhibitors during electropolishing in-ortho-phosphoric acid. *J. Mol. Liq.* 2021, *328*, 115421.

9. Fouda A. S., Elmorsi M., Shaban S. M., Fayed T., Azazy O. Evaluation of N-(3-(dimethyl hexadecyl ammonio)propyl) palmitamide bromide as cationic surfactant corrosion inhibitor for API N80 steel in acidic environment. *Egypt. J. Pet.* 2018, *27*, 683–694.

10. Quraishi M. A., Chauhan D. S., Ansari F. A. Development of environmentally benign corrosion inhibitors for organic acid environments for oil-gas industry. *J. Mol. Liq.* 2021, *329*, 115514.

11. Shaban S. M., Fouda A. S., Rashwan S. M., Ibrahim H. E., Elbhrawy M. F. Inhibitive action of new synthesized cationic surfactant with free hydroxyl group on the C1018 steel corrosion: experimental and theoretical investigations. *Prot. Met. Phys. Chem. Surf.* 2018, *54*, 709–723.

12. Aslam R., Mobin M., Zehra S., Obot I. B., Ebenso E. E. N,N′-Dialkylcystine Gemini and monomeric N-alkyl cysteine surfactants as corrosion inhibitors on mild steel corrosion in 1 M HCl solution: a comparative study. *ACS Omega* 2017, *2*, 5691–5707.

13. Winkler D. A., Breedon M., Hughes A. E., Burden F. R., Barnard A. S., Harvey T. G., Cole I. Towards chromate-free corrosion inhibitors: structure–property models for organic alternatives. *Green Chem.* 2014, *16*, 3349–3357.

14. Aiad I., Shaban S. M., Elged A. H., Aljoboury O. H. Cationic surfactant based on alignate as green corrosion inhibitors for the mild steel in 1.0 M HCl. *Egypt. J. Pet.* 2018, *27*, 877–885.

15. Shaban S., Fouda A. E., Elmorsi M., Fayed T., Azazy O. A study on the effect of new prepared amide cationic amphipathic on the corrosion inhibition of API N80 steel pipelines in oil wells industries. *Anti-Corros. Methods Mater.* 2018, *65*, 197–209.

16. Palomar-Pardavé M., Romero-Romo M., Herrera-Hernández H., Abreu-Quijano M., Likhanova N. V., Uruchurtu J., Juárez-García J. Influence of the alkyl chain length of 2 amino 5 alkyl 1,3,4 thiadiazole compounds on the corrosion inhibition of steel immersed in sulfuric acid solutions. *Corros. Sci.* 2012, *54*, 231–243.

17. Xia J., Zana R., Eds. *Gemini Surfactants: Synthesis, Interfacial and Solution-Phase Behavior, and Applications*, 1st ed; CRC Press: Boca Raton, 2003.

18. Abd-ElHamid A., El-dougdoug W., Syam S., Aiad I., Shaban S. M., Kim D. H. Synthesis of Gemini cationic surfactants-based pyridine Schiff base for steel corrosion and sulfate reducing bacteria mitigation. *J. Mol. Liq.* 2023, *369*, 120890.

19. Labena A., Hamed A., Ismael E. H. I., Shaban S. M. Novel Gemini cationic surfactants: thermodynamic, antimicrobial susceptibility, and corrosion inhibition behavior against acidithiobacillus ferrooxidans. *J. Surfactants Deterg.* 2020, *23*, 991–1004.

20. Gao Z., Tai S., Zhang Q., Zhao Y., Lü B., Ge Y., Huang L., Tang X. Synthesis and surface activity of biquaternary ammonium salt Gemini surfactants with ester bond. *Wuhan Univ. J. Nat. Sci.* 2008, *13*, 227–231.

21. Garcia M. T., Ribosa I., Kowalczyk I., Pakiet M., Brycki B. Biodegradability and aquatic toxicity of new cleavable betainate cationic oligomeric surfactants. *J. Hazard. Mater.* 2019, *371*, 108–114.
22. Stjerndahl M., Holmberg K. Synthesis and chemical hydrolysis of surface-active esters. *J. Surfactants Deterg.* 2003, *6*, 311–318.
23. Shaban S. M., Ismael E. H., Elsharif A. M., Elged A. H., El Basiony N. Preparation Gemini non-ionic surfactants-based polyethylene oxide with variable hydrophobic tails for controlling the catalytic and antimicrobial activity of AgNPs. *J. Mol. Liq.* 2022, *367*, 120416.
24. Friedli F. E., Keys R., Toney C. J., Portwood O., Whittlinger D., Doerr M. Novel new ester quaternaries for improved performance benefits as rinse cycle fabric softeners. *J. Surfactants Deterg.* 2001, *4*, 401–405.
25. Ma Y., Yue Y., Zhang H., Cheng F., Zhao W., Rao J., Luo S., Wang J., Jiang X., Liu Z., Liu N., Gao Y. 3D synergistical MXene/reduced graphene oxide aerogel for a piezoresistive sensor. *ACS Nano* 2018, *12*, 3209–3216.
26. Pisárčik M., Polakovičová M., Markuliak M., Lukáč M., Devínsky M. Self-assembly properties of cationic Gemini surfactants with biodegradable groups in the spacer. *Molecules* 2019, *24*, 1481–1494.
27. Shaban S. M., Abd-Elaal A. A. Studying the silver nanoparticles influence on thermodynamic behavior and antimicrobial activities of novel amide Gemini cationic surfactants. *Mater. Sci. Eng. C* 2017, *76*, 871–885.
28. Elgendy A., Elkholy A., El-Basiony N., Migahed M. Monte Carlo simulation for the antiscaling performance of Gemini ionic liquids. *J. Mol. Liq.* 2019, *285*, 408–415.
29. El-Basiony N., Sadeek S., Reda A., Migahed M. Experimental study for the carbon steel corrosion mitigation effect of the prepared trimeric cationic surfactant in 1M HCl. *Egypt. J. Chem.* 2021, *64*, 1927–1939.
30. Lakbaibi Z., Damej M., Molhi A., Benmessaoud M., Tighadouini S., Jaafar A., Benabbouha T., Ansari A., Driouich A., Tabyaoui M. Evaluation of inhibitive corrosion potential of symmetrical hydrazine derivatives containing nitrophenyl moiety in 1M HCl for C38 steel: experimental and theoretical studies. *Heliyon* 2022, *8*, e09087.
31. El-Basiony N. M., Elgendy A., El-Tabey A. E., Al-Sabagh A., El-Hafez G. A., El-raouf M. A., Migahed M. Synthesis, characterization, experimental and theoretical calculations (DFT and MC) of ethoxylated aminothiazole as inhibitor for X65 steel corrosion in highly aggressive acidic media. *J. Mol. Liq.* 2020, *297*, 111940.
32. Dohare K. R. A. P., Quraishi M. A., Obot I. B. Pyranpyrazole derivatives as novel corrosion inhibitors for mild steel useful for industrial pickling process: experimental and quantum chemical study. *J. Ind. Eng. Chem.* 2017, *52*, 197–210.
33. El-Tabei A. S., El-Tabey A. E., El-Basiony N. M. Newly imine-azo dicationic amphiphilic for corrosion and sulfate-reducing bacteria inhibition in petroleum processes: laboratory and theoretical studies. *Appl. Surf. Sci.* 2022, *573*, 151531.
34. Sliem M. H., El-Basiony N. M., Zaki E. G., Sharaf M. A., Abdullah A. M. Corrosion inhibition of mild steel in sulfuric acid by a newly synthesized schiff base: an electrochemical, DFT, and Monte Carlo simulation study. *Electroanalysis* 2020, *32*, 3145–3158.
35. Radwan A. B., Sliem M. H., Okonkwo P. C., Shibl M. F., Abdullah A. M. Corrosion inhibition of API X120 steel in a highly aggressive medium using stearamidopropyl dimethylamine. *J. Mol. Liq.* 2017, *236*, 220–231.
36. Berrissoul A., Ouarhach A., Benhiba F., Romane A., Guenbour A., Outada H., Dafali A., Zarrouk A. Exploitation of a new green inhibitor against mild steel corrosion in HCl: experimental, DFT and MD simulation approach. *J. Mol. Liq.* 2022, *349*, 118102.

37. El-Tabei A. S., Hegazy M., Bedair A., El-Basiony N., Sadeq M. Novel macrocyclic cationic surfactants: synthesis, experimental and theoretical studies of their corrosion inhibition activity for carbon steel and their antimicrobial activities. *J. Mol. Liq.* 2022, *345*, 116990.

38. Sliem M. H., Radwan A. B., Mohamed F. S., Alnuaimi N. A., Abdullah A. M. An efficient green ionic liquid for the corrosion inhibition of reinforcement steel in neutral and alkaline highly saline simulated concrete pore solutions. *Sci. Rep.* 2020, *10*, 14565.

39. Zaher A., Aslam R., Lee H. S., Khafouri A., Boufellous M., Alrashdi A. A., El-Aoufir Y., Lgaz H., Ouhssine M. A combined computational & electrochemical exploration of the Ammi visnaga L. extract as a green corrosion inhibitor for carbon steel in HCl solution. *Arab. J. Chem.* 2022, *15*, 103573.

40. El-Haddad M. A. M., Radwan A. B., Sliem M. H., Hassan W. M. I., Abdullah A. M. Highly efficient eco-friendly corrosion inhibitor for mild steel in 5 M HCl at elevated temperatures: experimental & molecular dynamics study. *Sci. Rep.* 2019, *9*, 3695.

41. Shaban S. M., Elsharif A. M., Elged A. H., Eluskkary M., Aiad I., Soliman E. Some new phospho-zwitterionic Gemini surfactants as corrosion inhibitors for carbon steel in 1.0 M HCl solution. *Environ. Technol. Innov.* 2021, *24*, 102051.

42. Elged A. H., Shaban S. M., Eluskkary M., Aiad I., Soliman E., Elsharif A. M., Kim D. H. Impact of hydrophobic tails of new phospho-zwitterionic surfactants on the structure, catalytic, and biological activities of AgNPs. *J. Ind. Eng. Chem*. 2021, *94*, 435–447.

43. Abd-Elaal A. A., Elbasiony N., Shaban S. M., Zaki E. Studying the corrosion inhibition of some prepared nonionic surfactants based on 3-(4-hydroxyphenyl) propanoic acid and estimating the influence of silver nanoparticles on the surface parameters. *J. Mol. Liq.* 2018, *249*, 304–317.

44. Mobin M., Aslam R. Experimental and theoretical study on corrosion inhibition performance of environmentally benign non-ionic surfactants for mild steel in 3.5 % NaCl solution. *Process Saf. Environ.* 2018, *114*, 279–295.

45. Deyab M. A. Enhancement of corrosion resistance in MSF desalination plants during acid cleaning operation by cationic surfactant. *Desalination* 2019, *456*, 32–37.

46. Zhou T., Yuan J., Zhang Z., Xin X., Xu G. The comparison of imidazolium Gemini surfactant [C14-4-C14im]Br2 and its corresponding monomer as corrosion inhibitors for A3 carbon steel in hydrochloric acid solutions: experimental and quantum chemical studies. *Colloid. Surf. A* 2019, *575*, 57–65.

47. Zhu Y., Free M. L., Woollam R., Durnie W. A review of surfactants as corrosion inhibitors and associated modeling. *Prog. Mater. Sci*. 2017, *90*, 159–223.

48. Azzam E. M. S., El-Salam H. M. A., Mohamed R. A., Shaban S. M., Shokry A. Control the corrosion of mild steel using synthesized polymers based on polyacrylamide. *Egypt. J. Pet.* 2018, *27*, 897–910.

49. Fouda A. S., Rashwan S., Shaban S. M., Ibrahim H. E., Elbhrawy M. Evaluation of a novel cationic surfactant based on 2-(2 (dimethylamino)ethoxy)ethanol as a corrosion inhibitor for carbon steel 1018 in 1.0MHCl solution. *Egypt. J. Pet.* 2018, *27*, 295–306.

50. Aiad I., Shaban S. M., El-Sukkary M. M., El-Awady M. Y., Soliman E. A. Electrical and gravimetric estimation of the corrosion inhibition of three synthesized cationic surfactants N-(3-(Butylidene amino) propyl)-N, N-dimethyl alkan-1-ammonium bromide derivatives in 1 M HCl. *Mater. Perform. Charact.* 2017, *6*, 429–450.

51. Prabhu R. A., Venkatesha T., Shanbhag A., Kulkarni G., Kalkhambkar R. Inhibition effects of some Schiff's bases on the corrosion of mild steel in hydrochloric acid solution. *Corros. Sci*. 2008, *50*, 3356–3362.

52. Badr E. A., Hefni H. H., Shafek S., Shaban S. M. Synthesis of anionic chitosan surfactant and application in silver nanoparticles preparation and corrosion inhibition of steel. *Int. J. Biol. Macromol.* 2020, *157*, 187–201.

53. Mishrif M. R., El-Din M. R. N., Khamis E. A. Utilization of ethoxylated pentamine oleamide as new Gemini surfactants for corrosion inhibition effectiveness in 1 M HCl solution. *Egypt. J. Pet.* 2018, *27*, 1357–1370.

54. Fawzy A., Abdallah M., Zaafarany I., Ahmed S., Althagafi I. Thermodynamic, kinetic and mechanistic approach to the corrosion inhibition of carbon steel by new synthesized amino acids-based surfactants as green inhibitors in neutral and alkaline aqueous media. *J. Mol. Liq.* 2018, *265*, 276–291.

55. Shamsheera K. O., Prasad A. R., Jaseela P., Joseph A. Effect of surfactant addition to Guar Gum and protection of mild steel in hydrochloric acid at high temperatures: experimental and theoretical studies. *J. Mol. Liq.* 2021, *331*, 115807.

56. Hegazy M. A., Awad M., Shawky M. Chemical, electrochemical, theoretical (DFT & MEP), thermodynamics and surface morphology studies of carbon steel during gas and oil production using three novel di-cationic amphiphiles as corrosion inhibitors in acidic medium. *J. Mol. Liq.* 2021, *337*, 116541.

57. Aslam R., Mobin M., Aslam J., Lgaz H., Chung I. M. Inhibitory effect of sodium carboxymethylcellulose and synergistic biodegradable Gemini surfactants as effective inhibitors for MS corrosion in 1 M HCl. *J. Mater. Res. Technol.* 2019, *8*, 4521–4533.

58. Feng L., Yin C., Zhang H., Li Y., Song X., Chen Q., Liu H. Cationic Gemini surfactants with a bipyridyl spacer as corrosion inhibitors for carbon steel. *ACS Omega* 2018, *3*, 18990–18999.

59. Shafek S. H., Ghiaty E. A., El-Basiony N. M., Badr E. A., Shaban S. M. Preparation of zwitterionic ionic surfactants-based sulphonyl for steel protections: experimental and theoretical insights. *Z. Phys. Chem.* 2023, *237*, 1–33.

60. Flores E. A., Olivares O., Likhanova N. V., Domínguez-Aguilar M. A., Nava N., Guzman-Lucero D., Corrales M. Sodium phthalamates as corrosion inhibitors for carbon steel in aqueous hydrochloric acid solution. *Corros. Sci.* 2011, *53*, 3899–3913.

61. Gao M., Zhang J., Liu Q., Li J., Zhang R., Chen G. Effect of the alkyl chain of quaternary ammonium cationic surfactants on corrosion inhibition in hydrochloric acid solution. *C. R. Chim.* 2019, *22*, 355–362.

62. Aslam R., Mobin M., Aslam J., Lgaz H., Chung I. M., Zehra S. Synergistic inhibition behavior between rhodamine blue and cationic Gemini surfactant on mild steel corrosion in 1 M HCl medium. *J. Mol. Struct.* 2021, *1228*, 129751.

63. Shaban S. M., Elbhrawy M., Fouda A., Rashwan S., Ibrahim H. E., Elsharif A. M. Corrosion inhibition and surface examination of carbon steel 1018 via N-(2-(2-hydroxyethyl)ethyl)-N,N-dimethyloctan-1-aminium bromide in 1.0 M HCl. *J. Mol. Struct.* 2021, *1227*, 129713.

64. Mobin M., Aslam R., Salim R., Kaya S. An investigation on the synthesis, characterization and anti-corrosion properties of choline based ionic liquids as novel and environmentally friendly inhibitors for mild steel corrosion in 5 % HCl. *J. Colloid Interface Sci.* 2022, *620*, 293–312.

65. Sliem M. H., Afifi M., Radwan A. B., Fayyad E. M., Shibl M. F., Heakal F. E. T., Abdullah A. M. AEO7 surfactant as an eco-friendly corrosion inhibitor for carbon steel in HCl solution. *Sci. Rep.* 2019, *9*, 2319.

66. Priscilla S. J., Judi V. A., Daniel K. S. R., Sivaji K. Effects of chromium doping on the electrical properties of ZnO nanoparticles. *Emerg. Sci. J.* 2020, *4*, 82–88.

67. Rahimi A., Farhadian A., Berisha A., Shaabani A., Varfolomeev M. A., Mehmeti V., Zhong X., Yousefzadeh S., Djimasbe R. Novel sucrose derivative as a thermally stable inhibitor for mild steel corrosion in 15 % HCl medium: an experimental and computational study. *Chem. Eng. J.* 2022, *446*, 136938.

68. Sliem M. H., Kannan K., Maurya M. R., Jlassi K., Sadasivuni K. K., Kumar B., Abdullah A. M. Rational synthesis of mixed metal oxide clusters supported on a partially etched MAX phase for efficient electrocatalytic CO2 conversion. *Top. Catal.* 2022, *21*, 1–16.

69. El-Basiony N. M., Elgendy A., Nady H., Migahed M. A., Zaki E. G. Adsorption characteristics and inhibition effect of two Schiff base compounds on corrosion of mild steel in 0.5 M HCl solution: experimental, DFT studies, and Monte Carlo simulation. *RSC Adv.* 2019, *9*, 10473–10485.
70. Fouda A. E., El-Aal A. A., Sliem M., Abdullah A. Caprylamidopropyl betaine as a highly efficient eco-friendly corrosion inhibitor for API X120 steel in 1 M H2SO4. *Egypt. J. Chem.* 2020, *63*, 759–776.
71. Shahzad K., Sliem M. H., Shakoor R. A., Radwan A. B., Kahraman R., Umer M. A., Manzoor U., Abdullah A. M. Electrochemical and thermodynamic study on the corrosion performance of API X120 steel in 3.5 % NaCl solution. *Sci. Rep.* 2020, *10*, 4314.
72. Abdelwedoud B. O., Damej M., Tassaoui K., Berisha A., Tachallait H., Bougrin K., Mehmeti V., Benmessaoud M. Inhibition effect of N-propargyl saccharin as corrosion inhibitor of C38 steel in 1 M HCl, experimental and theoretical study. *J. Mol. Liq.* 2022, *354*, 118784.
73. El-Tabei A. S., El-Azabawy O., El-Basiony N., Hegazy M. Newly synthesized quaternary ammonium bis-cationic surfactant utilized for mitigation of carbon steel acidic corrosion; theoretical and experimental investigations. *J. Mol. Struct.* 2022, *1262*, 133063.
74. Sliem M. H., Shahzad K., Sivaprasad V., Shakoor R., Abdullah A. M., Fayyaz O., Kahraman R., Umer M. A. Enhanced mechanical and corrosion protection properties of pulse electrodeposited NiP-ZrO$_2$ nanocomposite coatings. *Surf. Coat. Technol.* 2020, *403*, 126340.
75. Zhang X., Zhang M., Zhang Z., Lv R., Wu W. Bis-Mannich bases as effective corrosion inhibitors for N80 steel in 15 % HCl medium. *J. Mol. Liq.* 2022, *347*, 117957.
76. El-Wanees S. A., El-Basiony N., Al-Sabagh A., Alsharif M., El-Haleem S. A., Migahed M. Controlling of H2 gas production during Zn dissolution in HCl solutions. *J. Mol. Liq.* 2017, *248*, 943–952.
77. Li X., Deng S., Fu H. Triazolyl blue tetrazolium bromide as a novel corrosion inhibitor for steel in HCl and H$_2$SO$_4$ solutions. *Corros. Sci.* 2011, *53*, 302–309.
78. El-Basiony N. M., Badr E. E., Baker S. A., El-Tabei A. Experimental and theoretical (DFT&MC) studies for the adsorption of the synthesized Gemini cationic surfactant based on hydrazide moiety as X-65 steel acid corrosion inhibitor. *Appl. Surf. Sci.* 2021, *539*, 148246.